

Metasurface electron optics in graphene

Ruihuang Zhao,^{1,*} Pengcheng Wan,^{1,*} Ling Zhou,¹ Di Huang,¹ Haiqin Guo,¹ Hao Xia,¹ and Junjie Du^{1,†}

¹*State Key Laboratory of Precision Spectroscopy, School of Physics and Electronic Science,
East China Normal University, Shanghai 200062, China*

(Dated: April 28, 2022)

For electron optics in graphene, the propagation effect has so far been the only physical mechanism available. The resulting electron-optics-based components are large in size and operate at low temperatures to avoid violating the ballistic transport limits. In this paper, Dirac fermion metasurfaces, electronic counterparts of optical metasurfaces, are introduced for graphene electronics. By a metasurface, formally a linear array of gate-bias-controlled circular quantum dots, the wavefront of electron beams can be shaped within a one-quantum-dot-diameter distance, far below the ballistic limits at room temperature. This provides opportunities to create electron-optics-based devices that operate under ambient conditions. Moreover, unlike optical metasurfaces, Dirac fermion metasurfaces have near-perfect operating efficiencies and their high tunability allows for free and fast switching among functionalities. The concept of metasurface electron optics might open up a promising avenue for improving the performance of quantum devices in Dirac fermion materials.

* These authors contributed equally to this work.

† phyjunjie@gmail.com

Low energy graphene electrons behave like light because of their light-like dispersion and the ballistic transport[1]. Electron optics in semiconductor structures can be naturally extended to graphene. Both naturally-occurring and non-naturally-occurring optical phenomena such as the Goos-Hanchen shift[2], self-collimation[3], whispering-gallery modes[4–8], and negative-index[9–12] and zero-index[13] behaviors, have been reproduced by graphene electrons. Accordingly, various optics-inspired functional units, such as two-dimensional electron microscopes[14, 15], quantum switches[16–18], Fabry-Pérot cavities[19], electron waveguides[20–22], splitters[23, 24] and Veselago lenses[10–12], have been demonstrated. However, these remarkable achievements were made by following procedures used for bulk optical materials where wavefront shaping is accomplished via light propagation over a distance much larger than the wavelength. The propagation effect dictates that the optics-inspired electronic components are large in size. But, even if the large size of devices can be tolerated, the required long propagation distances often challenge the ballistic transport limits. To avoid violating these ballistic transport limits, these components have been designed to operate at low temperature since the mean free path of graphene electrons, $l = \mu\sqrt{\rho/\pi}h/2e$, which determines the ballistic transport limit, becomes larger at low temperature with enhanced carrier mobility μ [25].

The emergence of optical metasurfaces[26, 27] and metagratings[28, 29] opens the door to flat optics technology characterized by a single layer of nanoparticles. Wavefront shaping in optical metasurfaces is achieved over the scale of the free-space wavelength or on a smaller scale by introducing abrupt changes in phase or amplitude, following the generalized Snell’s law[26, 30]. This is fundamentally different from conventional diffractive optics based on the propagation effect. A single-particle-layer material not only greatly simplifies the fabrication process and lowers the loss in contrast to bulk materials, but also can mould optical wavefronts into shapes that are designed at will[30]. Inspired by the compactness features and the remarkable capabilities of wavefront engineering, we explore the possibility of realizing Dirac fermion metasurfaces in graphene, aiming to develop ultrasmall optics-inspired transistors that can operate under ambient conditions. In addition to the inherent advantages of metasurfaces such as compactness, low loss and easy-fabrication, it is shown that Dirac fermion metasurfaces also possess other remarkable properties such as near-perfect operating efficiency and high tunability, properties that are difficult to achieve in their optical counterparts. Also worth noting is that Dirac fermion metagratings have been explored in graphene and successfully produces unit-efficiency beam deflection through a near-180° angle over a distance much smaller than the electron wavelength[31].

RESULTS AND DISCUSSION

Formally, a Dirac fermion metasurface is a linear array of gate-bias-controlled circular quantum dots (QDs). The QDs are responsible for providing the required phase response in constructing a constant gradient of phase jump. The phase response capability of QDs is related to their “refractive index” which is defined as $n_s = (E - V_s)/E$ where E is the incident energy and V_s the applied bias[32]. For the electron scattering problem in the single valley case (see Supplemental Material), the low-energy electron dynamics can be described by the Dirac-Hamiltonian[32–38]

$$H = -i\hbar v_F \nabla \sigma + V_s \Theta(R_s - r), \quad (1)$$

which is analogous to the light scattering problem of an infinite dielectric cylinder. The Mie scattering method used widely in optics is applicable to graphene electrons; some of the results predicted by the method have been experimentally verified[39]. QDs with radius R_s are denoted as a step potential in Eq. (1) with the Heaviside step function $\Theta(R_s - r)$. The potential is smooth on the scale of the graphene’s intrinsic lattice constant but sharp on the scale of de Broglie wavelength, so the intervalley scattering is negligible. Meanwhile, theoretical studies have also shown that the QDs have nearly the same electron scattering behaviors[40] for the gradual transition of potentials smaller than $0.5R_s$.

As is well known, the behavior of a wave in a metasurface follows the generalized Snell’s law of refraction[26]

$$n_t \sin \theta_t - n_i \sin \theta_i = \frac{1}{k_0} \frac{d\Phi}{dx}, \quad (2)$$

where k_0 is the magnitude of the free space wavevector, θ_i and θ_t are, respectively, the angle of incidence and refraction, and n_i and n_t are the respective “refractive indices” of media on the incident and transmission sides of the metasurface. The phase gradient $d\Phi/dx$ implies an effective wavevector (equivalently, an effective momentum) along the interface that is produced and is imparted to the transmitted and reflected electrons. Thus the transmitted and reflected electron beams can be deflected through arbitrary angles, depending on the direction and magnitude of the phase gradient. The phase gradient is created within a unit cell consisting of several QDs to which the linearly increasing biases V_s are respectively applied. The variation of bias indicates the difference in “refractive index” between the QDs and thus the difference in phase response of electron waves. Figure 1 illustrates a linear phase distribution of the scattering fields in a unit cell composed of ten QDs. Throughout this paper, the energy of the incident electron beams is chosen to be $E = 65.82$ meV and the radius of the QDs to be 5 nm, with a spacing $d = 14.6$ nm between them. So the period of the metasurface is in Fig. 1 is $\Gamma = 9d = 131.4$ nm; in this figure the biases are given above each scattering field plot. Figure 1 shows that a complete phase coverage from 0 to 2π is obtained with an approximately

constant phase difference $\Delta\phi = \pi/5$ between neighbors. Thus the magnitude of the introduced wavevector in the x direction is $k_x^{add} = d\Phi/dx = 2\pi/\Gamma = 0.048/\text{nm}$. When a normal-incidence electron beam impinges on the metasurface, the transmitted beam will be bent at an angle $\theta_{calc} = \arctan(k_x^{add}/k_0)$, where k_0 is the magnitude of the free space wavevector with $n_i = n_t = 1$. This is simulated in Fig. 2(a), and the travel direction of the transmitted beam agrees well with the calculated bending angle $\theta_{calc} = 25^\circ$. Note that the scattering field of each QD in Fig. 1 is calculated by considering the inter-QD coupling interaction and employing multiple scattering theory[31, 41, 42](see also Supplemental Material). This ensures that the constant gradient of phase jumps really exists in the metasurface since the scattering field of an isolated QD may be very different from that of the same QD in a linear array.

A unit cell which covers the entire $0-2\pi$ range can also be composed of different numbers of QDs by adjusting only the bias while keeping the array invariant. We denote the number of the QDs in a unit cell by m_{unit} . A decrease of m_{unit} implies a larger phase gradient and also a larger introduced wavevector. Figures 2(b)-(f) show the bending of the electron beams by metasurfaces with $m_{unit}=9, 8, 7, 6$, and 5 . The bending angle increases gradually from Fig. 2(b) to (f). In addition, the Dirac fermion metasurfaces show a remarkable property in Fig. 2, that electron waves can be bent with nearly perfect efficiency. This is strikingly different from optical metasurfaces, in which an efficiency near 100% is difficult to achieve. It shows that electrons can more easily react to the lateral momentum introduced by the phase gradient than can photons. Moreover, comparing the panels in Fig. 2 shows that the efficiency is closer to 100% in the case of the longer unit cells because electrons have more opportunities to react to the introduced lateral momentum. Finally, perfect efficiency cannot be divorced from the successful suppression of reflection in the metasurfaces (see Supplemental Material Figure S2).

To verify that the beam bending at various θ_{actu} in Fig. 2 can be well explained by the introduced wavevectors due to phase gradient, we made a comparison between the two for all the cases in Table I where $\tan\theta_{calc} = k_x^{add}/k_0$ and $\tan\theta_{actu}$ are given. Here $k_x^{add} = 2\pi/\Gamma = 2\pi/m_{unit}d$ and θ_{actu} is directly read from Fig.2. The calculated bending angles agree well with the actual ones for m_{unit} between 7 and 10, but there are distinct deviations for $m_{unit}=6$ and 5 . To make matters worse, a weak beam is transmitted to the left of the normal in the later two cases. In an effort to find the causes of these deviations, we examine the phase response of each quantum dot for the case of $m_{unit}=6$, as shown Fig.3(a). One can see that only the former five QDs contribute to the formation of the linear phase gradient, whereas the QD with $V_s=750$ meV has a phase that goes against the linear gradient change. Moreover, this QD and the next two QDs of $V_s=680$ meV and $V_s=400$ meV together form a phase gradient increasing in the opposite direction; hence a left-oriented wavevector is produced, as shown in Fig. 3(a). Thus a small portion of electrons will propagate on the

left side of the normal in Fig. 2(e). Accordingly, the magnitude of the introduced right-oriented wavenumber should be calculated in terms of the period $\Gamma' = 4d = 58.4\text{nm}$. The new $\tan \theta_{calc}$ calculated by $k_x^{add} = 2\pi/\Gamma'$ is equal to 1.075 and agrees well with $\tan \theta_{actu}$ in Table I. Similarly, the deviation in the case of $m_{unit}=5$ in Table I has the same cause (see Supplemental Material Figure S1).

Exploring the causes of deviations can help to improve the efficiency of metasurfaces. We note that the electron scattering of the QD of $V_s=750$ meV is weak in contrast to other QDs in the unit cell. So the scattering of the other QDs will hardly be impacted if this QD is removed from the unit cell. Such a unit cell is schematically shown in the lower panel in Fig. 3(b), and the phase distribution is given in Fig. 3(c). We see that the opposite phase gradient is eliminated and thus only a right-oriented wavevector is introduced. The electron density distribution displayed in Fig. 3(d) shows that the electron beam bends to the right side of the normal with near-unit efficiency when the QD of $V_s=750$ meV is removed.

Since two equal and oppositely directed phase gradients represent left- and right-oriented equal-magnitude wavevectors, we can introduce them simultaneously in a metasurface to design an ultrathin electron splitter. One simple route for splitters is to achieve a right-oriented wavevector by the unit cells in the right half of the array and a left-oriented wavevector by the unit cells in the left half. This can be implemented by applying the biases enhanced from left to right to the QDs in the unit cells in the right half, as shown in Fig. 2, and the same biases but enhanced in the opposite direction in the left half. The impinging beam is split into two sub-beams at various angles to each other, as demonstrated in Figs. 4(a)-(f). We see that the beams are split with nearly perfect efficiency again and the splitting ratio is 50-50 in all cases.

Three points are worth emphasizing in the model. First, all the results reported in this paper are obtained in the same linear array of QDs. Specifically, the radius of the QDs and the spacing between them remain invariant in all simulations and we only modulate the biases on the QDs to realize both beam bending and beam splitting at various angles. The fast switching time of bias systems allows for high modulation efficiency. Second, near-perfect efficiency is obtainable, fundamentally different from optical counterparts. The performance of optical metasurfaces is subject to the intrinsic nature of light. The introduced momentum through the phase gradient cannot be perceived by all the photons due to the absence of interaction between photons. Because electrons are distinct from photons, the Dirac fermion metasurfaces have near-perfect operating efficiency. Third, the 5-nm radius QDs used in our simulations fall within current experimental manufacturing tolerance[43–45]. Very recently, even smaller circular QDs with atomically sharp boundaries have been obtained in experiments[43–45]. The fabrication techniques of high-precision QDs makes

experimental realization of the metasurfaces feasible.

I. CONCLUSIONS

In summary, we have demonstrated theoretically the feasibility of realizing metasurfaces for graphene ballistic electrons. A simple metasurface is a linear array of quantum dots (QDs) of the same radius. Phase discontinuities, the essential ingredient of gradient metasurfaces, are acquired by applying difference biases to the QDs. Following the generalized Snell's law, the metasurface imposes a control over electrons in a rather compact way with wavefront shaping accomplished below the ballistic transport limit at room temperature. Such metasurfaces dramatically reduce the size of electron-optics-based components and enable them to get rid of the dependence on low temperature conditions. The two kinds of transistors we demonstrated, beam benders and beam splitters, are achieved in the same linear array of QDs and can be conveniently switched back and forth by tuning the biases applied to the QDs. Dirac fermion metasurfaces represent a promising way to develop more practical and accessible electron optics technologies.

-
- [1] A. K. Geim, and K. S. Novoselov, *The rise of graphene*, Nat. Mater. **6**, 183 (2007).
 - [2] C. W. J. Beenakker, R. A. Sepkhanov, A. R. Akhmerov, and J. Tworzydło, *Quantum Goos-Hänchen Effect in Graphene*, Phys. Rev. Lett. **102**, 146804 (2009).
 - [3] C.-H. Park, Y.-W. Son, L. Yang, M. L. Cohen, and S. G. Louie, *Electron beam supercollimation in graphene superlattices*, Nano Lett. **8**, 2920-2924 (2008).
 - [4] Y. Zhao, J. Wyrick, F. D. Natterer, J. F. Rodriguez-Nieva, C. Lewandowski, K. Watanabe, T. Taniguchi, L. S. Levitov, N. B. Zhitenev, and J. A. Stroscio, *Creating and probing electron whispering-gallery modes in graphene*, Science **348**, 672-675 (2015).
 - [5] Y. Jiang, J. Mao, D. Moldovan, M. R. Masir, G. Li, K. Watanabe, T. Taniguchi, F. M. Peeters, and E. Y. Andrei, *Tuning a circular p-n junction in graphene from quantum confinement to optical guiding*, Nat. Nanotech. **12**, 1045-1049 (2017).
 - [6] F. Ghahari, D. Walkup, C. Gutiérrez, J. F. Rodriguez-Nieva, Y. Zhao, J. Wyrick, F. D. Natterer, W. G. Cullen, K. Watanabe, T. Taniguchi, L. S. Levitov, N. B. Zhitenev, and J. A. Stroscio, *An on/off Berry phase switch in circular graphene resonators*, Science **356**, 845-849 (2017).
 - [7] P. Hewageegana, and V. Apalkov, *Electron localization in graphene quantum dots*, Phys. Rev. B **77**, 245426 (2008).
 - [8] J. H. Bardarson, M. Titov, and P. W. Brouwer, *Electrostatic confinement of electrons in an integrable graphene quantum dot*, Phys. Rev. Lett. **102**, 226803 (2009).
 - [9] V. V. Cheianov, V. Fal'ko, and B. L. Altshuler, *The focusing of electron flow and a Veselago lens in graphene pn junctions*, Science **315**, 1252-1255 (2007).
 - [10] S. Chen, Z. Han, M. M. Elahi, K. M. M. Habib, L. Wang, B. Wen, Y. Gao, T. Taniguchi, K. Watanabe, J. Hone, A. W. Ghosh, and C. R. Dean, *Electron optics with p-n junctions in ballistic graphene*, Science **353**, 1522-1525 (2016).
 - [11] G.-H. Lee, G.-H. Park, and H.-J. Lee, *Observation of negative refraction of Dirac fermions in graphene*, Nat. Phys. **11**, 925-929. (2015).
 - [12] B. Brun, N. Moreau, S. Somanchi, V.-H. Nguyen, K. Watanabe, T. Taniguchi, J.-C. Charlier, C. Stampfer, and B. Hackens, *Imaging Dirac fermions flow through a circular Veselago lens*, Phys. Rev. B **100**, 041401(R) (2019).
 - [13] Y. Ren, P. Wan, L. Zhou, R. Zhao, Q. Wang, D. Huang, H. Guo, and J. Du, *Zero-index metamaterials for Dirac fermion in graphene*, Phys. Rev. B **103**, 085431 (2021).
 - [14] P. BøGgild, J. M. Caridad, C. Stampfer, G. Calogero, N. R. Papior, and M. Brandbyge, *A two-dimensional Dirac fermion microscope*, Nat. Commun. **8**, 15789 (2017).
 - [15] A. W. Barnard, A. Hughes, A. L. Sharpe, K. Watanabe, T. Taniguchi, and D. Goldhaber-Gordon, *Absorptive pinhole collimators for ballistic Dirac fermions in graphene*, Nat. Commun. **8**, 15418 (2017).

- [16] K. Wang, M. M. Elahi, L. Wang, K. M. M. Habib, T. Taniguchi, K. Watanabe, J. Hone, A. W. Ghosh, G.-H. Lee, and P. Kim, *Graphene Transistor Based on Tunable Dirac Fermion Optics*, Proc. Nat. Acad. Sci. **116**, 6575-6579 (2019).
- [17] R. N. Sajjad, and A. W. Ghosh, *High efficiency switching using graphene based electron “optics”*, Appl. Phys. Lett. **99**, 123101 (2011).
- [18] Q. Wilmart, S. Berrada, D. Torrin, V. H. Nguyen, G. Fève, J.-M. Berroir, P. Dollfus, and B. Plaçais, *A Klein-tunneling transistor with ballistic graphene*, 2D Mater. **1**, 011006 2014
- [19] A. V. Shytov, M. S. Rudner, and L. S. Levitov, *Klein backscattering and Fabry-Prot interference in graphene heterojunctions*, Phys. Rev. Lett. **101**, 156804 (2008).
- [20] J. R. Williams, T. Low, M. S. Lundstrom, and C. M. Marcus, *Gate-controlled guiding of electrons in graphene*, Nat. Nanotechnol. **6**, 222-225 (2011).
- [21] M. Kim, J.-H. Choi, S.-H. Lee, K. Watanabe, T. Taniguchi, S.-H. Jhi, and H.-J. Lee, *Valley-symmetry-preserved transport in ballistic graphene with gate-defined carrier guiding*, Nat. Phys. **12**, 1022-1026 (2016).
- [22] M.-H. Liu, C. Gorini, and K. Richter, *Creating and Steering Highly Directional Electron Beams in Graphene*, Phys. Rev. Lett. **118**, 066801 (2017).
- [23] P. Brandimarte, *A tunable electronic beam splitter realized with crossed graphene nanoribbons*, J. Chem. Phys. **146**, 199902 (2017).
- [24] J. Li, R. Zhang, Z. Yin, J. Zhang, K. Watanabe, T. Taniguchi, C. Liu, and J. Zhu, *A valley valve and electron beam splitter*, Science **362**, 1149 (2018).
- [25] A. S. Mayorov, R. V. Gorbachev, S. V. Morozov, L. Britnell, R. Jalil, L. A. Ponomarenko, P. Blake, K. S. Novoselov, K. Watanabe, T. Taniguchi, and A. K. Geim, *Micrometer-Scale Ballistic Transport in Encapsulated Graphene at Room Temperature*, Nano Lett. **11**, 2396 (2011).
- [26] N. Yu, P. Genevet, M. A. Kats, F. Aieta, J.-P. Tetienne, F. Capasso, and Z. Gaburro, *Light propagation with phase discontinuities: Generalized laws of reflection and refraction*, Science **334**, 333-337 (2011).
- [27] X. Ni, N. K. Emani, A. V. Kildishev, A. Boltasseva, and V. M. Shalae, *Broadband light bending with plasmonic nanoantennas*, Science **335**, 427 (2012).
- [28] J. J. Du, Lin, Z. F. Lin, S. T. Chui, W. L. Lu, H. Li, A. M. Wu, Z. Sheng, J. Zi, X. Wang, S. C. Zou, F. W. Gan, *Optical Beam Steering Based on the Symmetry of Resonant Modes of Nanoparticles*, Phys. Rev. Lett., **106**, 203903 (2011).
- [29] J. J. Du, Z. F. Lin, S. T. Chui, G. J. Dong, W. P. Zhang, *Nearly Total Omnidirectional Reflection by a Single Layer of Nanorods*, Phys. Rev. Lett. **110**, 163902 (2013).
- [30] N. Yu, and F. Capasso, *Flat optics with designer metasurfaces*, Nat. Mater. **13**, 139-150 (2014).
- [31] P. Wan, Y. Ren, Q. Wang, D. Huang, L. Zhou, H. Guo, and J. Du, *Dirac fermion metagratings in graphene*, npj 2D Materials and Applications **5**, 42 (2021).

- [32] R. L. Heinisch, F. X. Bronold, and H. Fehske, *Mie scattering analog in graphene:lensing, particle confinement, and depletion of Klein tunneling*, Phys. Rev. B **87**, 155409 (2013).
- [33] M. I. Katsnelson, F. Guinea, and A. K. Geim, *Scattering of electrons in graphene by clusters of impurities*, Phys. Rev. B **79**, 195426 (2009).
- [34] P. M. Ostrovsky, I. V. Gornyi, and A. D. Mirlin, *Electron transport in disordered graphene*, Phys. Rev. B **74**, 235443 (2006).
- [35] M. Hentschel, and F. Guinea, *Orthogonality catastrophe and kondo effect in graphene*, Phys. Rev. B **76**, 115407 (2007).
- [36] D. S. Novikov, *Elastic scattering theory and transport in graphene*, Phys. Rev. B **76**, 245435 (2007).
- [37] A. Pieper, R. L. Heinisch, and H. Fehske, *Scattering of two-dimensional Dirac fermions on gate-defined oscillating quantum dots*, Phys. Rev. B **91**, 045130 (2015).
- [38] J. Cserti, A. Pályi, and C. Péterfalvi, *Caustics due to a negative refractive index in circular graphene P-N junction*, Phys. Rev. Lett. **99**, 246801 (2007).
- [39] J. M. Caridad, S. Connaughton, C. Ott, H. B. Weber, and V. Krstić, *An electrical analogy to Mie scattering*, Nat. Commun. **7**, 12894 (2016).
- [40] A. Pieper, R. L. Heinisch, and H. Fehske, *Electron dynamics in graphene with gate-defined quantum dots*, Europhys. Lett. **104**, 47010 (2013).
- [41] Y. Ren, Y. Gao, P. Wan, Q. Wang, D. Huang, and J. Du, *Effective medium theory for electron waves in a gate-defined quantum dot array in graphene*, Phys. Rev. B **100** 045422 (2019).
- [42] Y. Tang, X. Y. Cao, R. Guo, Y. Y. Zhang, Z. Y. Che, F. T. Yannick, W. P. Zhang, and J.J. Du, *Flat-Lens Focusing of Electron Beams in Graphene*, Sci. Rep. **6**, 33522 (2016).
- [43] K. Bai, J. Zhou, Y. Wei, J. Qiao, Y. Liu, H. Liu, H. Jiang, and L. He, *Generating atomically sharp p-n junctions in graphene and testing quantum electron optics on the nanoscale*, Phys. Rev. B **97**, 045413 (2018).
- [44] C. Gutiérrez, L. Brown, C.-J. Kim, J. Park, and A. N. Pasupathy, *Klein tunnelling and electron trapping in nanometre-scale graphene quantum dots*, Nat. Phys. **12**, 1069-1075 (2016).
- [45] K. Bai, J. Qiao, H. Jiang, H. Liu, and L. He, *Massless Dirac fermions trapping in a quasi-one-dimensional npn junction of a continuous graphene monolayer*, Phys. Rev. B **95**, 201406(R) (2017).

TABLE I. Comparison between the calculated and actual bending angles for various m_{unit} .

m_{unit}	10	9	8	7	6	5
$\tan \theta_{calc}$	0.480	0.535	0.600	0.715	0.861	1.074
$\tan \theta_{actu}$	0.468	0.526	0.620	0.760	1.000	1.700

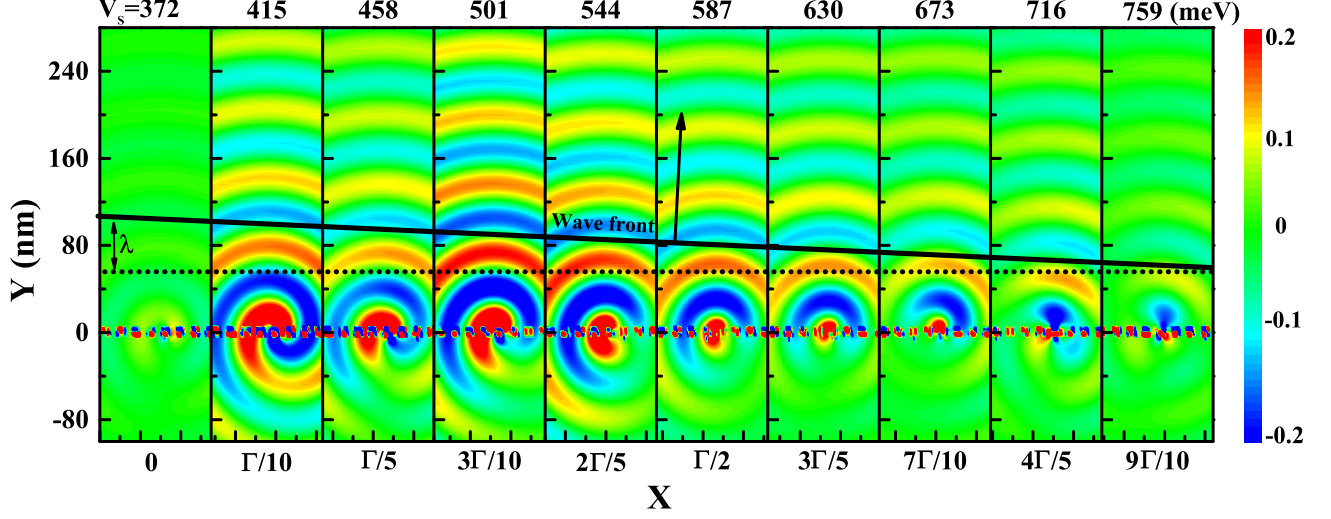


FIG. 1. **Formation of linear phase gradient.** The scattering field of the individual QDs constituting the unit cell of a metasurface. The tilted black straight line is the envelope of the projections of the cylindrical waves scattered by the QDs. A complete phase coverage from 0 to 2π is shown with an approximately constant phase difference $\Delta\phi = \pi/5$ between neighbors. The number of QDs in the unit cell is $m_{unit}=10$ and the biases V_s applied on each QD are given above each plot. The inter-QD coupling interaction has been considered in this calculation.

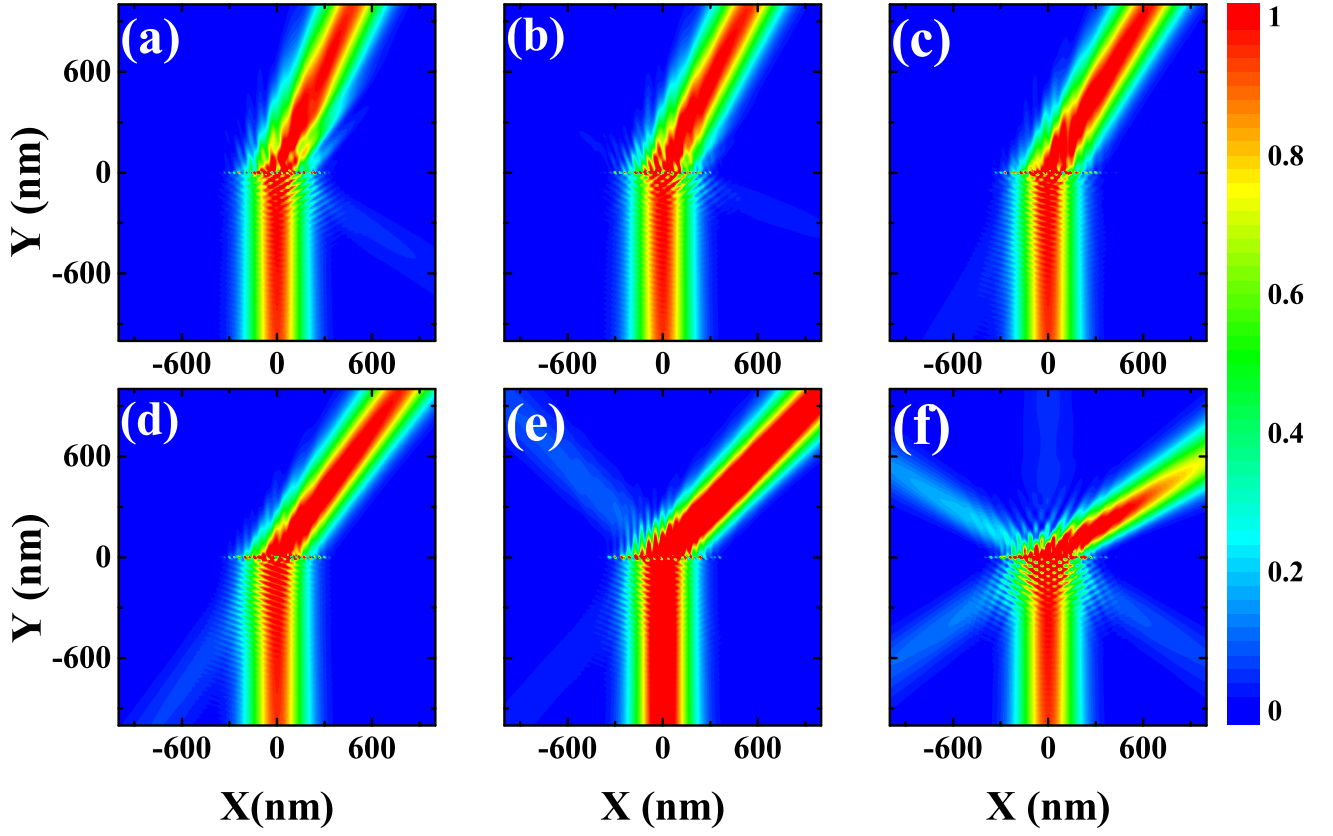


FIG. 2. **Simulation of beam bending.** The bending of electron beams after passing through the metasurface composed of unit cells with the number of QDs m_{unit} equal to (a) 10, (b) 9, (c) 8, (d) 7, (e) 6, and (f) 5. Linearly increasing biases with constant gradient are applied to the QDs in the unit cells. They are, respectively, $V_s=375, 420, 465, 510, 555, 600, 645, 690,$ and 735 meV for $m_{unit}=9$; $V_s=385, 440, 495, 550, 605, 660, 715,$ and 770 meV for $m_{unit}=8$; $V_s=385, 440, 495, 550, 605, 660,$ and 715 meV for $m_{unit}=7$; $V_s=400, 470, 540, 610, 680,$ and 750 meV for $m_{unit}=6$; and $V_s=390, 450, 510, 570,$ and 630 meV for $m_{unit}=5$.

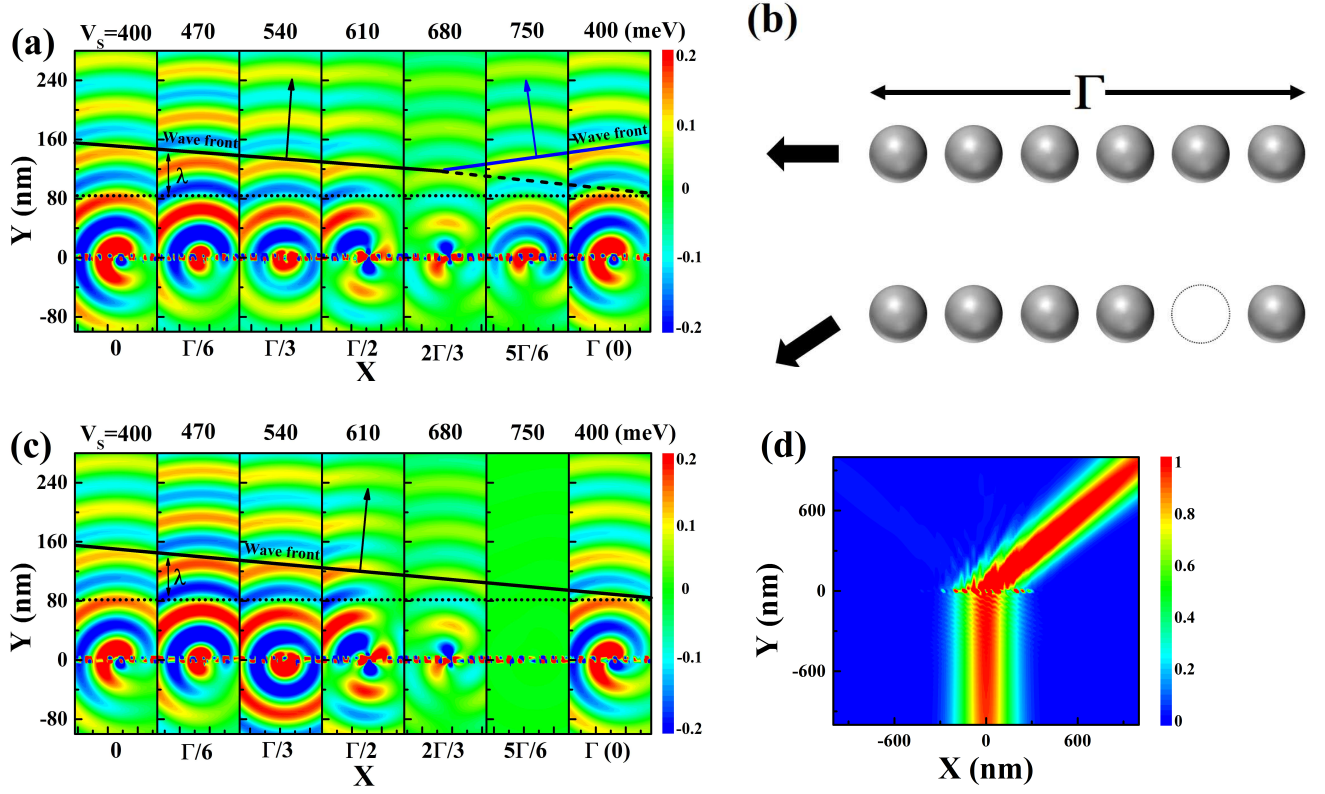


FIG. 3. **Illustration of the deviation at $m_{unit} = 6$ in Table I.** (a) The scattered field of the individual QDs in the presence of all six QDs. The tilted black and blue solid lines indicate, respectively, the desired and undesired phase gradients formed in the unit cell. (b) Schematics of the unit cells in the presence of all the QDs in the upper panel and in the absence of the QD of $V_s = 750$ meV in the lower panel. (c) The scattered field of the individual QDs with the QD of $V_s = 750$ meV removed. The phase gradient increasing in the opposite direction that appears in (a) is eliminated. (d) The beam bending occurring with near-unit efficiency when the QD of $V_s = 750$ meV is removed, in sharp contrast to Fig. 2(e).

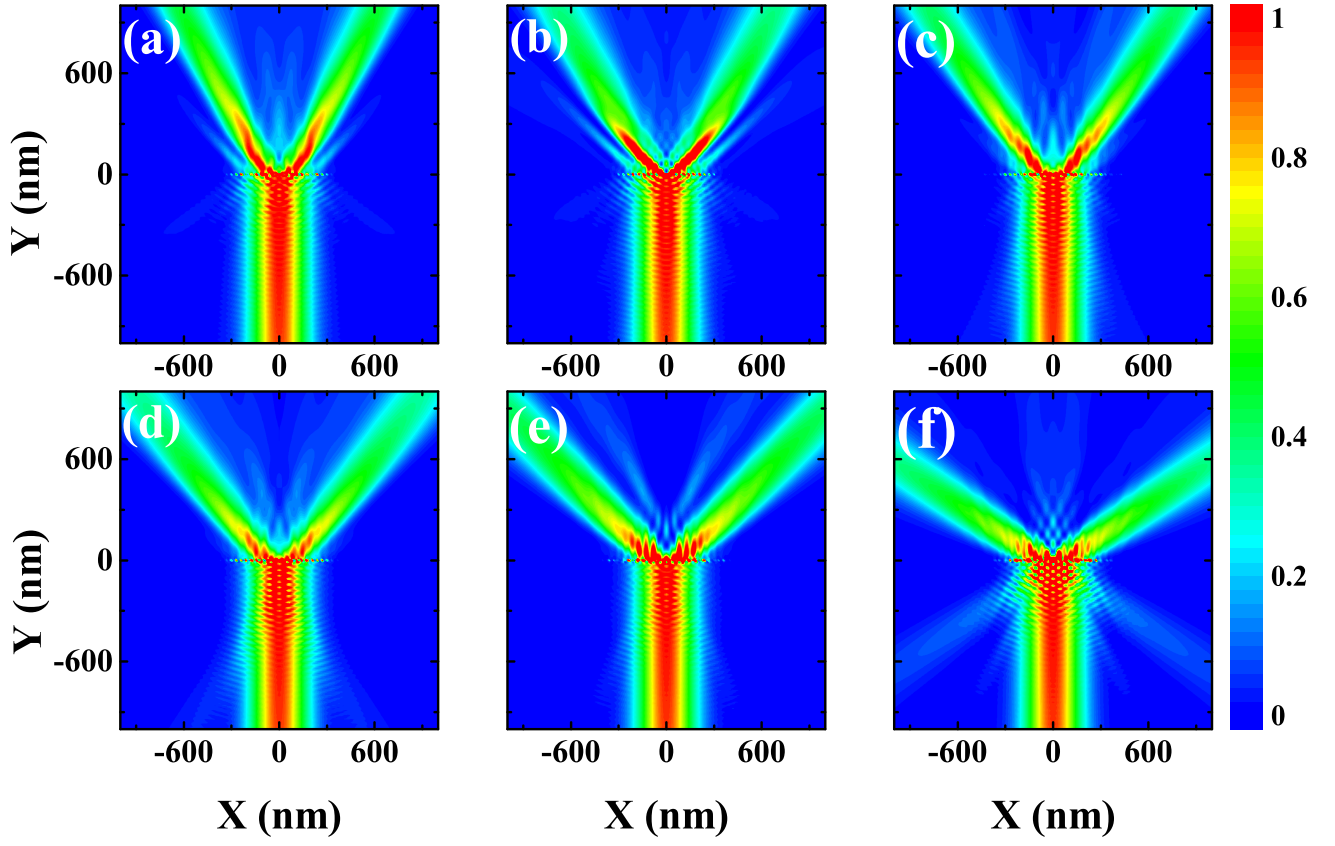


FIG. 4. **Simulation of beam splitting.** The splitting of electron beams after passing through metasurface composed of unit cells with the number of QDs m_{unit} equal to (a) 10, (b) 9, (c) 8, (d) 7, (e) 6, and (f) 5. The unit cells in the right half of the metasurfaces in (a)-(f) are the same as those in Fig.2(a)-(f), respectively, whereas the unit cells in the left half have the biases increasing in the opposite direction.